Geomechanics and Engineering, *Vol. 26, No. 5 (2021) 427-439*
https://doi.org/10.12989/gae.2021.26.5.427

A similarity solution for spherical cavity drained expansion in overconsolidated soils considering large deformation

Hanbo Zheng[1a], Hao Zhang*[2] and Fayun Liang[1b]

[1]*Department of Geotechnical Engineering, Tongji University, 1239 Siping Road, Yangpu District, Shanghai, P. R. China*
[2]*Department of Civil Engineering, Shanghai Normal University, 100 Haisi Road, Fengxian District, Shanghai, P. R. China*

(Received April 14, 2021, Revised August 4, 2021, Accepted August 17, 2021)

Abstract. This paper presents a novel similarity solution for drained spherical cavity expansion in overconsolidated soils, which creatively incorporates the large strain into similarity solution. The salient feature of the present solution lies in that it properly represents the large deformation associated responses of the overconsolidated soil during cavity expansion. The logarithmic strain components are reasonably incorporated into the similarity solution, which is a general solution technique that has been widely used to solve cavity expansion problems, to creatively account for the large deformation of soils during cavity expansion in such a solution framework. The competent modified unified-hardening (UH) model is employed to properly represent the unique behavior of overconsolidated soils during expansion, where three-dimensional strength characteristics of the soil are taken into account as well. The partial differential governing equations under Eulerian description are transformed into a set of first order ordinary differential equations under Lagrangian description and further solved as an initial value problem by MATLAB. The present method is verified by comparing with the modified Cam-clay model based solutions and an extensive parameter analysis is subsequently conducted for soils with different overconsolidation ratio. The unique expansion behaviors in the overconsolidated soils including the peak strength behavior, strain-hardening/softening and shear dilatancy behaviors are discussed in a comprehensive and in-depth manner.

Keywords: drained expansion; large deformation; overconsolidated soil; parameter analysis; similarity solution; spherical cavity

1. Introduction

The cavity opening problem has attracted extensive attention of scholars since Bishop *et al.* (1945) proposed an expansion solution in soil mass, which was subsequently applied to variety of geotechnical problems. In the last 50 years, various cavity expansion solutions for geotechnical materials are proposed by scholars and engineers, and these solutions mainly focus on two aspects. The first aspect of interest is adopting different assumptions and soil models in the cavity expansion analysis. In the early years, soil was assumed to perform linear-elasticity in the elastic region and perform perfect plasticity in the plastic region during expansion (Bigoni and Laudiero 1989, Coutinho 1990, Vaziri and Wang 1993). Subsequently, based on the critical state theory, the modified Cam-clay (MCC) model is adopted to reflect nonlinear elastoplastic behavior of the soil, and some analytical/semi-analytical solutions for cavity expansion are proposed (Davis *et al.* 1984, Collins and Stimpson 1994, Silvestri and Abou-Samra 2012, Sengun *et al.* 2014). With the development of soil constitutive theory in recent years, some advanced constitutive models such as the bounding surface models, unified hardening models and improved MCC models, have been adopted in the expansion analysis to consider the anisotropy (Sivasithamparam and Castro 2018, Li *et al.* 2019), unsaturated (Schnaid *et al.* 2004, Jiang *et al.* 2020, Yang *et al.* 2021) and overconsolidated behaviors (Ha *et al.* 2014, Wu and Xu 2020) of the soils.

The second aspect of interest is developing novel solution techniques of cavity expansion problems. Since Vesic *et al.* (1972) proposed the solution framework of cavity expansion in soil mass, a number of solution techniques have appeared in the next few years (Carter *et al.* 1979, Yu 1992, Collins and Stimpson 1994, Cao *et al.* 2002, Chen and Abousleiman 2013, Grevtsev 2013). Among them, Collins and his collaborators present a similarity solution technique for cavity created problem (expansion with zero initial radius), and the solution is further extended to analyze the finite cavity expansion problem (Collins and Stimpson 1994). Based on the self-similarity of cavity created problem, this similarity solution technique defines the velocity of soil particles during cavity expansion. The response of soil is described by governing equations under Eulerian description which further skillfully simplify and nondimensionalize by adopting an auxiliary variable. Due to its exceptional ability and adaptability, the similarity technique has become a general

*Corresponding author, Assistant Professor
E-mail: zhanghaotumu@163.com
[a]Ph.D. Student
E-mail: 1932350@tongji.edu.cn
[b]Professor
E-mail: fyliang@tongji.edu.cn

ISSN: 2005-307X (Print), 2092-6219 (Online)

solution for the cavity expansion problem, and has been adopted in a number of studies (Russell and Khalili 2002, Zhou *et al.* 2018, Zhang *et al.* 2020). However, above available similarity solutions are mostly developed based on the small stain assumption, while cavity expansion is a larger deformation problem in essential. With the expanding of the cavity radius, the soil particles expand outward significantly, showing the behavior of large deformation (Shuttle and Jefferies 2016), which is different from the small strain condition. Especially for overconsolidated soil, the soil response under large deformation is significantly different from that under small deformation (Konkol and Bałachowski 2017, Nguyen *et al.* 2020). The adoption of small strain assumption leads to overestimation of the stiffness of soil behavior in overconsolidated soils than that in normally consolidated soils, which may cause inaccurate calculation results of the ultimate state of cavity expansion (Vrakas 2016). Therefore, it is of great significance to obtain a similarity solution that considering the large strain behavior of cavity expansion in overconsolidated soils.

It is worth noting that overconsolidation is also one of the apparent characteristics of natural soil, a large number of field and laboratory tests demonstrate that most of the naturally deposited clayey soils have essentially over consolidation features (Yazdani and Toufigh 2012), which indicate the soils have unique stress histories and will present unique mechanical behaviors during cavity expansion, such as dilatancy behavior, peak strength behavior and so on (Oka *et al.* 2002, Hsieh *et al.* 2002, Frydman 2011, Jocković and Vukićević 2017, Jiang *et al.* 2020). However, due to the unreasonable shape of Hvorslev envelope, MCC model is insufficient to reflect the unique behaviors of overconsolidated soils, and the cavity expansion solutions based on MCC model may be not conservative enough which result in overestimation of soil strength (Yao *et al.* 2012). Comfortingly, Yao *et al.* (2012) proposed a modified unified-hardening (UH) model which can reasonably reflect the unique behaviors of overconsolidated soils by modifying the shape of Hvorslev envelope and adopting a reference yield surface, and Wu and Xu (2020) well proved the applicability of the model to the cavity opening problem in overconsolidated soil. Accordingly, the modified UH model may be a good choice to facilitate the developing of a similarity solution for large deformation based cavity expansion problem in overconsolidated soils.

The purpose of this paper is to propose a novel similarity solution of drained spherical cavity expansion in overconsolidated soils considering large deformation. The logarithmic strain is creatively adopted in the similarity solution technique to reflect the large deformation of soils. The stress transformation method based on Spatially Mobilized Plane (SMP) criterion is used to consider the 3D strength of soil, and the unique overconsolidated behaviors of soils are reflected by the modified UH model. Based on the drained condition, the partial differential equations (PDEs) under Eulerian description are transformed into a set of first order ordinary differential equations (ODEs) under Lagrangian description, and the governing equations is further solved by MATLAB as an initial value problem. It should be noted that drained condition means the specific volume of soil during cavity expansion is not constant and the stress path is unknown, which is significantly different from the undrained solution (Osinov and Cudmani 2001). Subsequently, the results are compared with a MCC model based-solution to show the particular expansion responses in overconsolidated soils, and an extensive parameter analysis is conducted for soils with different overconsolidation ratios. The applicability of present study to the analysis of cavity expansion in overconsolidated soils, especially in heavily overconsolidated soils is further discussed. The results obtained in this paper can be further applied to analyze the pile installation or the mechanism of cone penetration test (CPT) in overconsolidated soils under the drained or dried site condition.

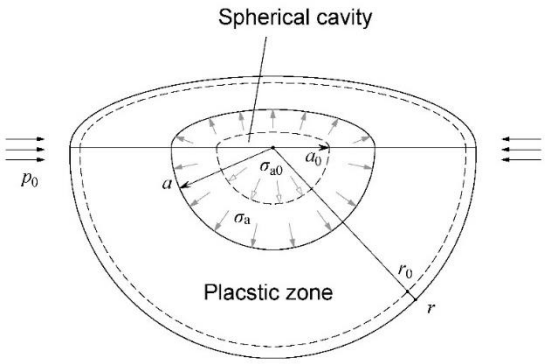

Fig. 1 Schematic illustration of spherical cavity expansion problem

2. Problem definition

2.1 Definition of spherical cavity expansion problem

The schematic illustration of a spherical cavity expansion problem in overconsolidated soils is shown in Fig. 1. In infinity space, the spherical cavity with radius a_0 is under an initial state with mean stress p_0 and soil specific volume v_0. With the internal cavity pressure increasing from its initial value σ_{a0} to σ_a, the radius of the cavity varying from a_0 to a. The radial coordinate of an arbitrary soil particle moving outward from r_0 to r and a plastic zone is formed in the soil adjacent to the spherical cavity.

Considering the geometric symmetry of the problem, the quasi-static stress state of an arbitrary soil element around the spherical cavity can be uniquely determined by the equilibrium equation along the radial direction alone, which gives:

$$\frac{\mathrm{d}\sigma_r'}{\mathrm{d}r} + 2\frac{\sigma_r' - \sigma_\theta'}{r} = 0 \tag{1}$$

where σ_r' and σ_θ' = the effective radial and circumferential stresses; r = the radial coordinate; $\frac{\mathrm{d}(\ )}{\mathrm{d}r}$ denotes the derivative with respect to the radial position for every particle at any moment, which is a Eulerian description.

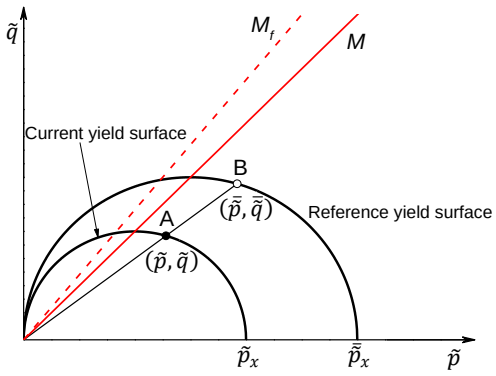

Fig. 2 Yield surfaces of Unified hardening model (Yao *et al.* 2012)

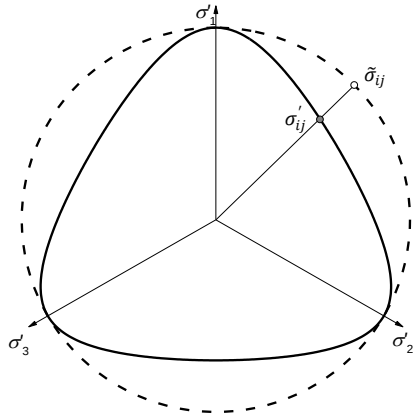

Fig. 3 Stress transformed method (modified from Yao *et al.* 2012)

2.2 Modified UH model for overconsolidated soils

In order to reflect the properties of overconsolidated soil reasonably, such as peak strength and strain hardening/softening characteristics, etc., the modified unified-hardening (UH) model, which was developed by Yao *et al.* (2012) and will be adopted in the present solution, is briefly described in this section, including plastic potential, yield surface, and hardening rules. The modified UH model is an improved model based on the original UH model by adopting a parabolic Hvorslev envelope rather than a straight one. The optimization of the envelope shape makes the model more suitable for the highly overconsolidated clay and reduces the number of parameters to be determined. The model parameters of modified UH model are the same as those of modified Cam-clay (MCC) model, which have explicit physical meanings and can be easily obtained by conventional triaxial tests.

As demonstrated in Fig. 2, two yield surfaces with similar shape but different hardening parameters are suggested by modified UH model. The current yield surface has similar form with MCC model but adopt a unified hardening parameter H. the expression of current yield surface is defined as follows (Yao *et al.* 2012):

$$f = g = \ln\frac{\tilde{p}}{\tilde{p}_x} + \ln\left(1 + \frac{\tilde{q}^2}{M^2\tilde{p}^2}\right) = \ln\frac{\tilde{p}}{\tilde{p}_{x0}} + \ln\left(1 + \frac{\tilde{q}^2}{M^2\tilde{p}^2}\right) - \frac{H}{c_p} = 0 \quad (2)$$

where f and g = the current yield function and plastic potential function; $\tilde{p}$ and $\tilde{q}$ = the mean effective stress and deviatoric stress in the transformed stress space, and expressed in Eq. (3); $\tilde{p}_x$ = intersection of the current yield surface with the $\tilde{p}$ (p) axis; $\tilde{p}_{x0}$ = the value of $\tilde{p}_x$ when $\varepsilon_v^p = 0$; M = the critical stress ratio; $c_p = \frac{\lambda-\kappa}{1+e_0}$; λ and κ = slopes of the isotropic compression line and swelling line respectively; e_0 = initial void ratio. respectively.

$$\tilde{p} = p = \frac{I_1}{3} \quad (3a)$$

$$\tilde{q} = \frac{2I_1}{3\sqrt{(I_1I_2 - I_3)/(I_1I_2 - 9I_3)} - 1} \quad (3b)$$

where $I_1 = \sigma'_1 + \sigma'_2 + \sigma'_3$, $I_2 = \sigma'_1\sigma'_2 + \sigma'_2\sigma'_3 + \sigma'_3\sigma'_1$ and $I_3 = \sigma'_1\sigma'_2\sigma'_3$; and σ'_1, σ'_2, σ'_3 = the effective major, intermediate and minor effective principal stress, respectively.

It should be noted that the modified UH model is defined in the transformed stress space aiming to consider the 3D strength of soil as shown in Fig. 3. Under this context, the following transformed stress tensor based on the SMP criterion is used (Yao *et al.* 2009)

$$\tilde{\sigma}_{ij} = p\delta_{ij} + \frac{q^*}{q}(\sigma_{ij} - p\delta_{ij}) \quad (4a)$$

$$q^* = \tilde{q} = \frac{2I_1}{3\sqrt{(I_1I_2 - I_3)/(I_1I_2 - 9I_3)} - 1} \quad (4b)$$

The other yield surface is called the reference yield surface which has same form with MCC model which adopt plastic volumetric strain ε_v^p as the hardening parameter and expressed as follows:

$$\bar{f} = \bar{g} = \ln\frac{\bar{\tilde{p}}}{\bar{\tilde{p}}_x} + \ln\left(1 + \frac{\bar{\tilde{q}}^2}{M^2\bar{\tilde{p}}^2}\right) = \ln\frac{\bar{\tilde{p}}}{\bar{\tilde{p}}_{x0}} + \ln\left(1 + \frac{\bar{\tilde{q}}^2}{M^2\bar{\tilde{p}}^2}\right) - \frac{\varepsilon_v^p}{c_p} = 0 \quad (5)$$

where $\bar{f}$ and $\bar{g}$ = the reference yield function and plastic potential function; $\bar{\tilde{p}}_x$ = the maximum value of $\tilde{p}_x$ within stress history.

The hardening parameter H of the current yield surface is defined as follows:

$$H = \int \mathrm{D}H = \int \frac{M_f^4 - \tilde{\eta}^4}{M^4 - \tilde{\eta}^4}\mathrm{D}\varepsilon_v^p \quad (6)$$

where $\tilde{\eta} = \tilde{q}/\tilde{p}$; $\mathrm{D}(\ ) =$ increment of variables; M_f = the potential peak stress ratio and expressed as (Yao *et al.* 2012):

$$M_f = 6\left[\sqrt{\frac{k}{R}\left(1 + \frac{k}{R}\right)} - \frac{k}{R}\right] \quad (7a)$$

$$k = \frac{M^2}{12(3 - M)} \quad (7b)$$

where R = overconsolidation parameter, which equals to the

reciprocal of the overconsolidation ratio *OCR*. Moreover, the parameter R can also be defined by the location dependence between point A and B on the current yield surface and the reference yield surface as shown in Fig. 2:

$$R = \frac{1}{OCR} = \frac{\tilde{p}_{\mathrm{x}}}{\bar{\tilde{p}}_{\mathrm{x}}} \tag{8}$$

and R varies with the change of the current yield surface. For overconsolidated soils, it is obvious that $R < 1$. According to Eq. (7), the potential peak stress ratio M_{f}, which reflect the peak strength characteristic of overconsolidated soils, is directly related to R. Moreover, M_{f} further determined the hardening parameter H directly, which controls the rate of hardening and softening of the current yield surface during loading (Yao *et al.* 2012, Wu and Xu 2020). When $R = 1$ indicates that soil has normal consolidation characteristics, and the current yield surface coincides with the reference yield surface, and the modified UH model degenerates to MCC model.

3. Solution of drained cavity expansion

3.1 Constitutive relation in modified UH model

Considering Hooke's law, the elastic increment relation can be expressed by Young's modulus E and Poisson's ratio v. The elastic matrix is given as

$$\begin{bmatrix} \acute{\varepsilon}_{\mathrm{r}}^{\mathrm{e}} \\ \acute{\varepsilon}_{\theta}^{\mathrm{e}} \end{bmatrix} = \begin{bmatrix} \frac{1}{E} & -2\frac{v}{E} \\ -\frac{v}{E} & \frac{1-v}{E} \end{bmatrix} \begin{bmatrix} \acute{\sigma}_r \\ \acute{\sigma}_{\theta} \end{bmatrix} \tag{9}$$

where $(\acute{})$ denotes the time derivative (rate) of a given material particle, which is a Lagrangian description defined as follows: following Collins and Stimpson (1994), a dimensionless radial coordinate ρ is given as

$$\rho = \frac{r}{r_p} = \frac{r}{Wt} \tag{10}$$

in which r_p = the position of the elastic-plastic region. The speed of expansion of the elastic-plastic boundary W can be taken as a constant.

For a physical quantity Θ, the local time and the space derivative for a given soil particle is first defined with respect to ρ as

$$(\dot{\Theta}) = \frac{\mathrm{d}(\Theta)}{\mathrm{d}t} = -W\frac{\rho}{r_p}\frac{\mathrm{d}(\Theta)}{\mathrm{d}\rho} \tag{11a}$$

$$\frac{\mathrm{d}(\Theta)}{\mathrm{d}r} = \frac{1}{r_p}\frac{\mathrm{d}(\Theta)}{\mathrm{d}\rho} \tag{11b}$$

Then the material time derivative can be expressed as

$$(\dot{\theta}) = (\dot{\Theta}) + w\frac{\mathrm{d}(\Theta)}{\mathrm{d}r} = \frac{W(\bar{w}-\rho)}{r_p}\frac{\mathrm{d}(\Theta)}{\mathrm{d}\rho} \tag{12}$$

where w = the speed of soil particle at r; and $\bar{w} = w/W$. It is worth noting that when solving the problem of cavity expansion problem based on modified UH model, it is considered that there is no pure elastic region in the soil. For overconsolidated soils, when cavity expansion occurs, the surrounding soil reaches the stage of elastic-plastic deformation immediately. The elastic strain components in different direction are calculated by Eq. (9), and the plastic strains in different direction are defined by the flow rule, which is given as:

$$\acute{\varepsilon}_{ij}^{\mathrm{p}} = \frac{\mathrm{D}\varepsilon_{ij}^{\mathrm{p}}}{\mathrm{D}t} = \acute{\Lambda}\frac{\mathrm{D}f}{\mathrm{D}\tilde{\sigma}_{ij}} \tag{13}$$

where $\acute{\Lambda}$ is a plastic scalar, which can be calculated by the consistency condition as follows:

$$\begin{aligned} \acute{f} &= \frac{Df}{D\tilde{\sigma}_{ij}}\acute{\tilde{\sigma}}_{ij} + \frac{Df}{DH}\frac{DH}{\mathrm{D}\varepsilon_{\mathrm{v}}^{\mathrm{p}}}\acute{\varepsilon}_{\mathrm{v}}^{\mathrm{p}} \\ &= \frac{Df}{D\tilde{\sigma}_{ij}}\acute{\tilde{\sigma}}_{ij} - \frac{1}{c_{\mathrm{p}}}\frac{M_{\mathrm{f}}^4 - \tilde{\eta}^4}{M^4 - \tilde{\eta}^4} \quad \acute{\varepsilon}_{\mathrm{v}}^{\mathrm{p}} = 0 \end{aligned} \tag{14}$$

qhere

$$\acute{\varepsilon}_{\mathrm{v}}^{\mathrm{p}} = \acute{\varepsilon}_1^{\mathrm{p}} + \acute{\varepsilon}_2^{\mathrm{p}} + \acute{\varepsilon}_3^{\mathrm{p}} = \acute{\Lambda}\frac{\partial f}{\partial \tilde{\sigma}_{ii}} \tag{15}$$

Therefore, substituting Eq. (15) into Eq. (14), $\acute{\Lambda}$ is calculated as:

$$\acute{\Lambda} = c_{\mathrm{p}}\frac{M^4 - \tilde{\eta}^4}{M_{\mathrm{f}}^4 - \tilde{\eta}^4}\frac{\frac{Df}{D\tilde{\sigma}_{ij}}\acute{\tilde{\sigma}}_{ij}}{\frac{Df}{D\tilde{\sigma}_{ii}}} \tag{16}$$

where

$$\begin{aligned} \frac{Df}{D\tilde{\sigma}_{ij}} &= \frac{\delta_{ij}}{3\tilde{p}} + \frac{M^2\tilde{p}^2}{M^2\tilde{p}^2 + \tilde{q}^2}\left(-2\frac{\tilde{q}^2}{M^2\tilde{p}^3}\right)\frac{\delta_{ij}}{3} + \frac{M^2\tilde{p}^2}{M^2\tilde{p}^2 + \tilde{q}^2}2\frac{\tilde{q}}{M^2\tilde{p}^2}\frac{3(\tilde{\sigma}_{ij} - \tilde{p}\delta_{ij})}{2\tilde{q}} \\ &= \frac{1}{M^2\tilde{p}^2 + \tilde{q}^2}\left[\frac{\delta_{ij}}{3\tilde{p}}(M^2\tilde{p}^2 - \tilde{q}^2) + 3(\tilde{\sigma}_{ij} - \tilde{p}\delta_{ij})\right] \end{aligned} \tag{17a}$$

$$\frac{Df}{D\tilde{\sigma}_{ii}} = \frac{M^2\tilde{p}^2 - \tilde{q}^2}{(M^2\tilde{p}^2 + \tilde{q}^2)\tilde{p}} \tag{17b}$$

Substituting Eq. (16) into Eq. (13), the relationship between plastic strain component and stress component can be given in matrix form:

$$\begin{bmatrix} \acute{\varepsilon}_{\mathrm{r}}^{\mathrm{p}} \\ \acute{\varepsilon}_{\theta}^{\mathrm{p}} \end{bmatrix} = \begin{bmatrix} \frac{a_{\mathrm{r}}^2}{K_{\mathrm{p}}} & 2\frac{a_{\mathrm{r}}a_{\theta}}{K_{\mathrm{p}}} \\ \frac{a_{\mathrm{r}}a_{\theta}}{K_{\mathrm{p}}} & 2\frac{a_{\theta}^2}{K_{\mathrm{p}}} \end{bmatrix} \begin{bmatrix} \acute{\tilde{\sigma}}_{\mathrm{r}} \\ \acute{\tilde{\sigma}}_{\theta} \end{bmatrix} \tag{18}$$

It should be noted that the elastic matrix defines a relation between strain rate and original stress rate, while Eq. (18) is formulated between strain rate and transformed stress rate. Therefore, the transformed stress rate should be converted to original stress rate to unify the form of stress components as:

$$\begin{bmatrix} \acute{\tilde{\sigma}}_{\mathrm{r}} \\ \acute{\tilde{\sigma}}_{\theta} \end{bmatrix} = \begin{bmatrix} c_{\mathrm{rr}} & 2c_{\mathrm{r}\theta} \\ c_{\theta\mathrm{r}} & 2c_{\theta\theta} \end{bmatrix} \begin{bmatrix} \acute{\sigma}_r \\ \acute{\sigma}_{\theta} \end{bmatrix} \tag{19}$$

where c_{ij} $(i,j = r,\theta)$ = the equation parameters directly determined by the stress component. The expression of c_{ij} is given in the appendix.

Hence, combining Eqs. (18) and (19), the plastic strain-

stress increment relationship can be calculated as:

$$\begin{bmatrix}\acute{\varepsilon}_{\mathrm{r}}^{\mathrm{p}}\\ \acute{\varepsilon}_{\theta}^{\mathrm{p}}\end{bmatrix}=\begin{bmatrix}\frac{a_{\mathrm{r}}^2}{K_{\mathrm{p}}} & 2\frac{a_{\mathrm{r}}a_{\theta}}{K_{\mathrm{p}}}\\ \frac{a_{\mathrm{r}}a_{\theta}}{K_{\mathrm{p}}} & 2\frac{a_{\theta}^2}{K_{\mathrm{p}}}\end{bmatrix}\begin{bmatrix}\acute{\tilde{\sigma}}_{\mathrm{r}}\\ \acute{\tilde{\sigma}}_{\theta}\end{bmatrix}=\begin{bmatrix}\frac{a_{\mathrm{r}}^2}{K_{\mathrm{p}}} & 2\frac{a_{\mathrm{r}}a_{\theta}}{K_{\mathrm{p}}}\\ \frac{a_{\mathrm{r}}a_{\theta}}{K_{\mathrm{p}}} & 2\frac{a_{\theta}^2}{K_{\mathrm{p}}}\end{bmatrix}\begin{bmatrix}c_{\mathrm{rr}} & 2c_{\mathrm{r}\theta}\\ c_{\theta\mathrm{r}} & 2c_{\theta\theta}\end{bmatrix}\begin{bmatrix}\acute{\sigma}_{r}\\ \acute{\sigma}_{\theta}\end{bmatrix} \quad (20)$$

Combining Eqs. (9) and (20), the relationship between elastic and plastic stress-strain can obtained:

$$\begin{bmatrix}\acute{\varepsilon}_{\mathrm{r}}\\ \acute{\varepsilon}_{\theta}\end{bmatrix}=\begin{bmatrix}\acute{\varepsilon}_{\mathrm{r}}^{\mathrm{p}}+\acute{\varepsilon}_{\mathrm{r}}^{\mathrm{e}}\\ \acute{\varepsilon}_{\theta}^{\mathrm{p}}+\acute{\varepsilon}_{\theta}^{\mathrm{e}}\end{bmatrix}=\begin{bmatrix}\frac{1}{E}+c_{\mathrm{rr}}\frac{a_{\mathrm{r}}^2}{K_{\mathrm{p}}}+2c_{\theta\mathrm{r}}\frac{a_{\mathrm{r}}a_{\theta}}{K_{\mathrm{p}}} & -2\frac{v}{E}+2c_{\mathrm{r}\theta}\frac{a_{\mathrm{r}}^2}{K_{\mathrm{p}}}+4c_{\theta\theta}\frac{a_{\mathrm{r}}a_{\theta}}{K_{\mathrm{p}}}\\ -\frac{v}{E}+c_{\mathrm{rr}}\frac{a_{\mathrm{r}}a_{\theta}}{K_{\mathrm{p}}}+2c_{\theta\mathrm{r}}\frac{a_{\theta}^2}{K_{\mathrm{p}}} & \frac{1-v}{E}+2c_{\mathrm{r}\theta}\frac{a_{\mathrm{r}}a_{\theta}}{K_{\mathrm{p}}}+4c_{\theta\theta}\frac{a_{\theta}^2}{K_{\mathrm{p}}}\end{bmatrix}\begin{bmatrix}\acute{\sigma}_{\mathrm{r}}'\\ \acute{\sigma}_{\theta}'\end{bmatrix} \quad (21)$$

where

$$a_k=\frac{1}{3\tilde{p}}(M^2\tilde{p}^2-\tilde{q}^2)+3(\tilde{\sigma}_k-\tilde{p});k=r,\theta \quad (22)$$

$$K_{\mathrm{p}}=\frac{1}{c_{\mathrm{p}}}\frac{M_{\mathrm{f}}^4-\tilde{\eta}^4}{M^2+\tilde{\eta}^2}\tilde{p} \quad (23)$$

Inversing Eq. (21), the incremental elastoplastic constitutive matrix given as:

$$\begin{bmatrix}\acute{\sigma}_{r}\\ \acute{\sigma}_{\theta}\end{bmatrix}=\begin{bmatrix}d_{11} & d_{12}\\ d_{21} & d_{22}\end{bmatrix}\begin{bmatrix}\acute{\varepsilon}_{\mathrm{r}}\\ \acute{\varepsilon}_{\theta}\end{bmatrix} \quad (24)$$

where d_{11}, d_{12}, d_{21} and d_{22} are the matrix coefficients, which are also given in appendix respectively.

3.2 Governing equations for spherical cavity problem

Considering the substantial displacement caused by the cavity expansion, large deformation theory is considered in the similarity solution technique, and the total radial, circumferential and volumetric strain components are defined as follows (Chen and Abousleiman 2013):

$$\varepsilon_r=-\ln\left(\frac{\mathrm{d}r}{\mathrm{d}r_0}\right) \quad (25a)$$

$$\varepsilon_\theta=-\ln\left(\frac{r}{r_0}\right) \quad (25b)$$

$$\varepsilon_v=\varepsilon_r+2\varepsilon_\theta=-\ln\left(\frac{v}{v_0}\right) \quad (25c)$$

Combing Eqs. (11) - (12) and Eq. (25), the derivative of radial, circumferential and volumetric strain with respect to the dimensionless radial coordinate ρ can be expressed as:

$$\frac{\mathrm{d}\varepsilon_r}{\mathrm{d}\rho}=-\frac{1}{\overline{w}-\rho}\frac{\mathrm{d}\overline{w}}{\mathrm{d}\rho} \quad (26a)$$

$$\frac{\mathrm{d}\varepsilon_\theta}{\mathrm{d}\rho}=-\frac{1}{\overline{w}-\rho}\frac{\overline{w}}{\rho} \quad (26b)$$

$$\frac{\mathrm{d}\varepsilon_v}{\mathrm{d}\rho}=-\frac{1}{v}\frac{\mathrm{d}v}{\mathrm{d}\rho} \quad (26c)$$

For the drained condition, combining Eqs. (11) and (12), (24) and (26), rewriting the stress rate components and strain rate components in the constitutive matrix, one has:

$$\begin{bmatrix}\frac{d\sigma_r}{d\rho}\\ \frac{d\sigma_\theta}{d\rho}\end{bmatrix}=\begin{bmatrix}d_{11} & d_{12}\\ d_{21} & d_{22}\end{bmatrix}\begin{bmatrix}-\frac{1}{v}\frac{dv}{d\rho}+2\frac{1}{\overline{w}-\rho}\frac{\overline{w}}{\rho}\\ -\frac{1}{\overline{w}-\rho}\frac{\overline{w}}{\rho}\end{bmatrix} \quad (27)$$

And the equilibrium equation (Eq. (1)) can be rewritten with the aid of Eq. (11) as

$$\frac{d\sigma_r}{d\rho}=-2\frac{\sigma_r-\sigma_\theta}{\rho} \quad (28)$$

Combining Eqs. (27) and (28), the derivative of soil specific volume to the dimensionless radial coordinate can derived as:

$$-2\frac{\sigma_r'-\sigma_\theta'}{\rho}=d_{11}\left(-\frac{1}{v}\frac{dv}{d\rho}+2\frac{1}{\overline{w}-\rho}\frac{\overline{w}}{\rho}\right)-\frac{d_{12}}{\overline{w}-\rho}\frac{\overline{w}}{\rho} \quad (29a)$$

$$\frac{dv}{d\rho}=2\frac{v}{d_{11}}\frac{\sigma_r'-\sigma_\theta'}{\rho}+\frac{2d_{11}-d_{12}}{d_{11}}\frac{v}{\overline{w}-\rho}\frac{\overline{w}}{\rho} \quad (29b)$$

Rewriting Eq. (26)

$$\frac{d\overline{w}}{d\rho}=\frac{\overline{w}-\rho}{v}\frac{dv}{d\rho}-2\frac{\overline{w}}{\rho} \quad (30)$$

3.3 Initial conditions for governing equations

Since the cavity expands in a self-similar way, the initial condition for any given material point should be the same as the far-field, which can be expressed as

$$\rho_{in}=\rho_p=1 \quad (31a)$$

$$v_{in}=v_0 \quad (31b)$$

$$\sigma_{rin}=\sigma_{\theta in}=p_0 \quad (31c)$$

$$\overline{w}_{in}=0 \quad (31d)$$

Then the governing equations Eqs. (27)-(29) of spherical cavity expansion problem are now formulated with respect to ρ, which can be solved as an initial value problem via MATLAB. The basic variable involved in this problem includes σ_{r}', σ_{θ}' and v.

The relation between expansion ratio $\frac{a}{a_0}$ and the circumferential strain at cavity wall can be given as:

$$\varepsilon_\theta(r=a)=-\ln\frac{a}{a_0} \quad (32)$$

The circumferential strain can also be obtained by integrating Eq. (26b) as:

$$\varepsilon_\theta(r=a)=-\int_{\rho_p}^{\rho_a}\frac{1}{\overline{w}-\rho}\frac{\overline{w}}{\rho}\mathrm{d}\rho \quad (33)$$

Combining Eqs. (32) and (33), one has:

$$\frac{a}{a_0}=\exp\left(\int_{\rho_p}^{\rho_a}\frac{1}{\overline{w}-\rho}\frac{\overline{w}}{\rho}\mathrm{d}\rho\right) \quad (34)$$

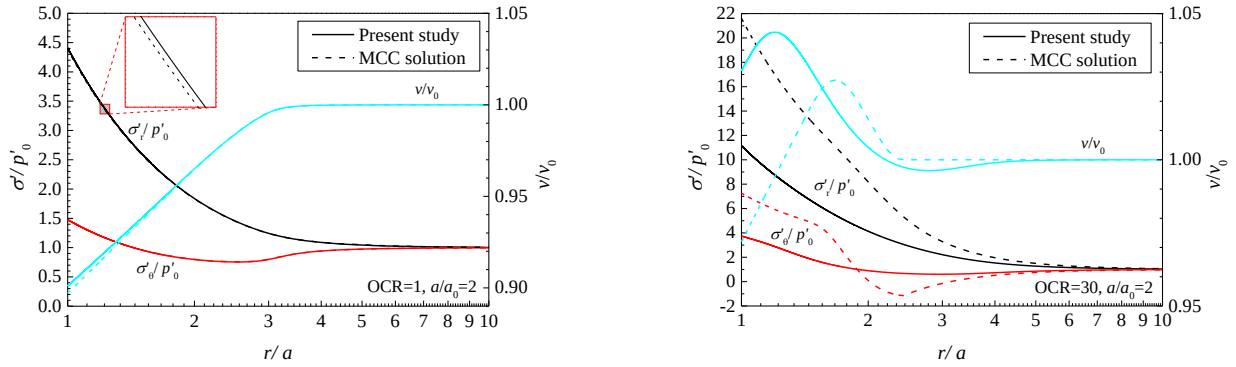

(a) OCR=1 (b) OCR=30

Fig. 4 Comparison between present study and MCC solution

After finding ρ_a from Eq. (34), the normalized radial coordinate of a given particle should be

$$\frac{r}{a} = \frac{\rho}{\rho_a} \tag{35}$$

4. Results and discussion

In this section, a series of numerical calculations are carried out for the spherical cavity expansion problem in Boston clay under different overconsolidated condition. Stress field in the vicinity of spherical cavity is calculated firstly based on the modified UH model, then the results are compared with those obtained by other scholars using MCC model. Both normally consolidated and heavily overconsolidated conditions are considered to verify the present method and further show the applicability for overconsolidated soils of the modified UH model. Furthermore, a comprehensive parameter analysis is carried out for seven different *OCR* values as shown in Table 1, where G_0 is the shear modulus of soil before expansion and defined by Eq. (36). The effects of *OCR* on the stress distribution, specific volume and stress path of the surrounding soil during spherical cavity expansion are studied, then the potential peak strength, strain hardening/softening and dilatancy behaviors of overconsolidated soils are discussed. The calculation in this paper adopts the soil parameters summarized by Chen and Abousleiman (2013), and on this basis, in order to show the unique properties of overconsolidated soils more vividly, three groups of soil parameters corresponding to the case of heavily overconsolidated soils are added as shown in Table 1.

$$G_0 = \frac{3(1-2v)vp_0}{2(1+v)\kappa} \tag{36}$$

4.1 Comparison with MCC solutions

Fig. 4 shows the comparative curves between result of present study and the MCC solution under different *OCR* values. The radial distribution curves of normalized stresses and normalized specific volume in the adjacent soil are plotted respectively, and normalized radial coordinate r/a in logarithmic form is adopted to describe the situation around the cavity wall more clearly. Note that the MCC solution adopted the spherical cavity drained expansion solution proposed by Rao *et al.* (2017), and two cases of $OCR = 1$ and $OCR = 30$ are calculated respectively. As shown in Fig. 4(a), for normally consolidated soils ($OCR = 1$). The radial stress component and tangential stress component reach their maximum values at cavity wall and return to their initial values in the far field. The specific volume decrease due to the densification of soil at cavity wall, and gradually increases to the initial value with the increase of radial coordinates. Apparently, the result curves of present study perfectly coincides with that of the MCC solution which verifies the present method. Fig. 4(a) also shows that the modified UH model is degraded to the MCC model when the soil is normally consolidated, i.e., the current yield surface coincides with the reference yield surface, and the overconsolidation parameter R remains constant and equals to 1 during cavity expansion process. Correspondingly, Fig. 4(b) compares the space distribution curves of stresses and specific volume under heavily overconsolidated condition ($OCR = 30$). As shown in the figure, the stress level at cavity wall is much higher than that of the normally consolidated condition, and the stress components reduce to their initial values with the radial coordinates increase. It is worth noting that the present study can reasonably reflect the shear dilatancy of soils when spherical cavity expands in the overconsolidated soils. In Fig. 4(b), the normalized specific volume v/v_0 at the cavity wall is larger than its initial value 1, which indicates

Table 1 Soil parameters used in parametric analysis

OCR	$\sigma'_r(\sigma'_\theta)$: kPa	p'_{x0}: kPa	v_0	G_0: kPa	$\overline{p}'_{x0}$: kPa
1	120	120	2.105	4388	120
1.2	120	120	2.06	4302	144
3	120	120	1.97	4113	360
5	120	120	1.91	3985	600
10	120	120	1.83	3812	1200
20	120	120	1.75	3639	2400
30	120	120	1.70	3537	3600

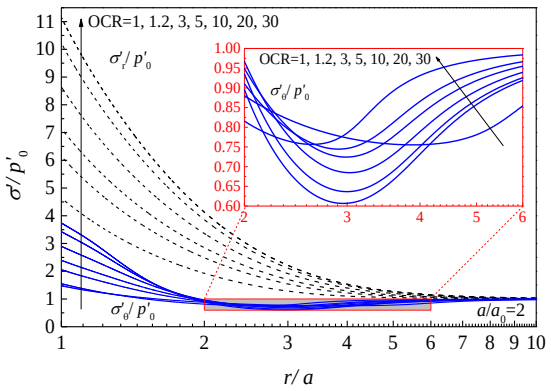

(a) Stress components

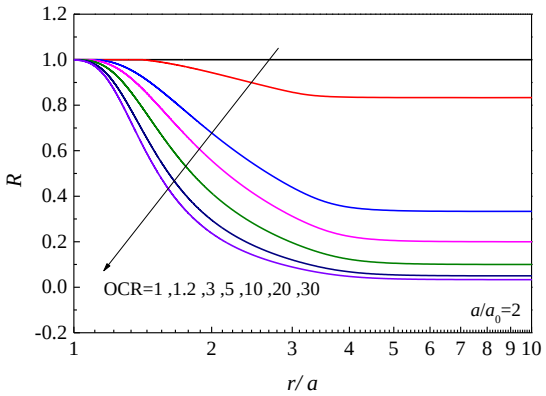

(b) Overconsolidation parameter

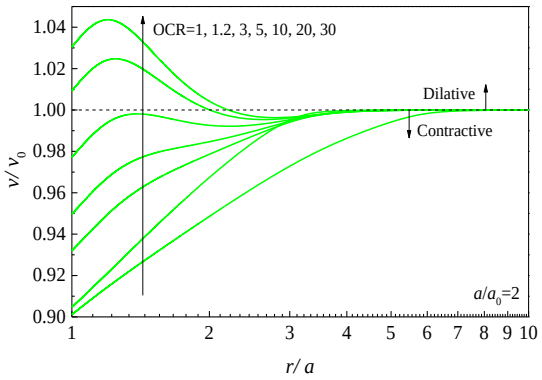

(c) Normalized specific volume

Fig. 5 Distribution curves of different variables versus dimensionless radial coordinates

that the volume of soil increase and the soil at cavity wall undergoes shear dilatancy during cavity expansion. With the increase of radial coordinates, v/v_0 first decreases to less than its initial value, and gradually increases back to 1, which indicates that shear contraction occurs in the soil at a distance from cavity wall. This is consistent with the results of a large number of laboratory tests and theoretical studies, that is, the higher *OCR* value, the larger volume dilatancy under shearing and the clayey soil is more prone to dilatation (Hattab and Hicher 2004, Wang and Wu 2021). However, the solution based on MCC model could not reasonably interpret the serious shear dilatancy of soil under extreme high *OCR* value, and the stress components of MCC solution are overestimated, especially at cavity wall. It should be noted that all kinds of unreasonable phenomena caused by using MCC solution will result in incorrect or even absurd results in the analysis of pile driving or cone penetration test in heavily overconsolidated soils, which means that the stress field in vicinity during expansion could not be calculated correctly and the unique properties of overconsolidated soils could not be reasonably interpreted. Therefore, a comprehensive parameter analysis of different *OCR* cases by the present method is carried out in next few paragraphs, and the characteristics of overconsolidated soils in the process of cavity expansion are discussed.

4.2 Effect of OCR on radial distribution of variables

Fig. 5 plots the radial distribution of stress components, overconsolidation parameter and specific volume in the adjacent soil respectively after the spherical cavity expansion with cavity wall displacement $a/a_0 = 2$, and seven cases of *OCR* = 1, 1.2, 3, 5, 10, 20 and 30 are taken into account to discuss the effect of the degree of overconsolidation. Fig. 5(a) shows the distribution curves of normalized stress components versus normalized radial coordinate r/a after cavity expansion for different oversolidated soils. As shown in the figure, the radial stress values of the cavity wall increase sharply compared with the initial state, and decrease gradually with the increase of radial coordinates until reaching the in situ stress. The larger the *OCR* value, the greater the radial stress component at the cavity wall, and the larger the range of soil around the spherical cavity affected by the expansion. In addition, the tangential stress component σ_θ also greater than its initial value at cavity wall. Interestingly, with r/a increases to more than about 2, σ_θ/p_0 reduce to less than the initial value 1, and further reaches to its minimum value at different radial coordinate for different overconsolidated soils, which means a tangential stress-reduced area has formed in the plastic zone around the spherical cavity. For the normally consolidated soil, the position where σ_θ/p_0 reduces to minimum value is about $r/a = 4.3$. However, σ_θ/p_0 reduces more rapidly and reaches minimum at the position of $r/a < 3$ for the overconsolidated soils. Moreover, the reduction of tangential stress decreases with the increase of *OCR*, which is a unique expansion response in overconsolidated soils.

Fig. 5(b) shows the radial distribution of

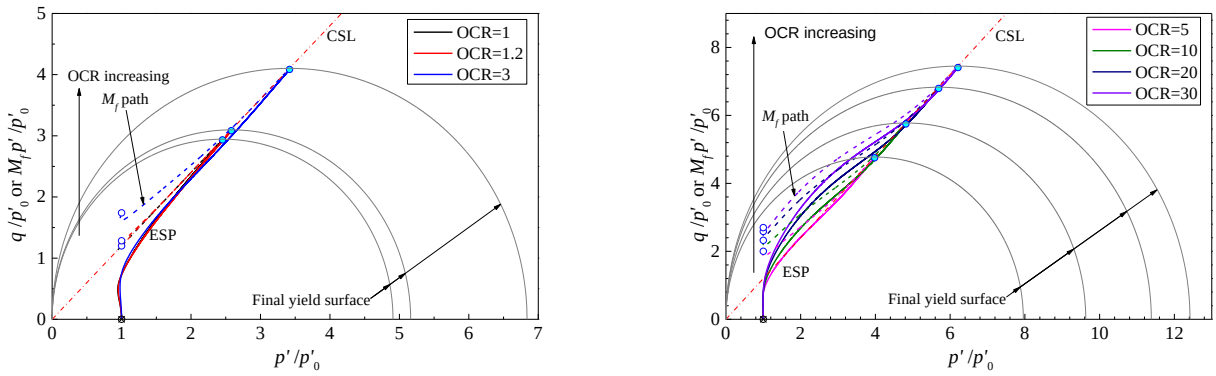

(a) Normally consolidated or slightly overconsolidated soils (b) Heavily overconsolidated soils

Fig. 6 Effective stress path and M_f path of given particle at cavity wall

overconsolidation parameter R with different OCR values. According to the definition of overconsolidation parameter given in Eq. (8), it is known that the change of R represents the relationship between the current stress state and the maximum stress level in the soil's history, which can be used to interpret the influence of cavity expansion on the soil particles at different positions. As shown in Fig. 5(b) that for normally consolidated soil, as expected, R is constant and equal to 1 during expansion, and therefore appears as a horizontal straight line in the figure. For the soils with $OCR > 1$, the overconsolidation parameters equal to their initial values $1/OCR$ in the far field ($r/a > 8$), and gradually increase to 1 with the decrease of r/a. These results indicate that the expansion of cavity causes the surrounding overconsolidated soils to approach the normally consolidated state, which is consistent with the phenomenon observed during the pile installation (Randolph and Wroth 1981). Moreover, the disturbed range of different overconsolidated soils can be reflected in this figure, that is, with the increase of OCR values, the radius of normally consolidated zone in the surrounding soil decrease and the initial descent rates of R values increase.

Fig. 5(c) shows the radial distribution of normalized specific volume v/v_0 for different overconsolidated soils. As is clearly shown in the figure, for the normally consolidated condition, the soil a cavity wall undergoes shear contraction during cavity expansion, and the soil particles are compacted, which resulting in a decrease of specific volume. With the position of soil particles away from the cavity wall, the specific volume gradually returns to its initial value. Furthermore, with the increase of OCR, the value of v/v_0 at the cavity wall is larger than that of normally consolidated soil, and even greater than 1 for extreme heavily overconsolidated soils ($OCR = 20$ or 30). This result indicates the soil at cavity wall and vicinity undergoes shear dilatancy, and the more heavily overconsolidation is, the more obvious shear dilatancy of the soil undergoes. With the increase of r/a, the value of v/v_0 reduce to less than 1, that is, the soil particles away from the cavity wall $(r/a > 2)$ undergo shear contraction. Moreover, it is interesting that after the cavity expansion in the normally consolidated soils, the specific volume of the soil is affected to a range of $r/a = 7$, while in the overconsolidated soils, the value is only about 4, which also is a unique expansion response in overconsolidated soils. It should note that due to the capabilities of the modified UH model for extreme heavily overconsolidated soils (Yao *et al.* 2012), the present method can be applied to the analysis of pile installation and cone penetration test in the soils with extremely high OCR conditions.

4.3 Effect of OCR on strain-hardening and softening behavior

Fig. 6 plots the effective stress path (ESP) and M_f path in $p' - q$ plane during the expansion of soil particles on the cavity wall from the initial state to the instant of $a/a_0 = 2$. Normalized mean effective stresses and normalized deviator stresses are adopted, and different OCR cases are take into account, then the results are separately plotted in subgraphs according to the degree of overconsolidation. The ESP of normally consolidated soil and slightly overconsolidated soils ($OCR = 1$, 1.2 and 3) are shown in Fig. 6(a). Before the cavity expansion, ESPs are located at the initial stress point on the isotropic consolidation line, with the cavity expansion, the surrounding soils enter the plastic state immediately. As shown in the figure, the ESPs reach to the critical state line (CSL) from below side, and in this process, the stress ratio η, i.e., the slope of ESPs increase monotonically, which indicates the soils undergo strain hardening. However, for the moderately or heavily overconsolidated soils ($OCR = 5$, 10, 20 and 30) as shown in Fig. 6(b), the ESPs show different results: the ESPs also start from the initial stress point, but soon reach and cross CSL to the upper left, and then intersect CSL from the upper side at the final yield surface. In this process, the stress ratio η first increases and then decreases, which indicates that the soil undergoes strain-hardening firstly and then occurs strain-softening after reaching its peak strength, which is also consistent with the results of a number of laboratory tests.

In Fig. 7, the variation of stress ratio η and volumetric strain ε_v with deviatoric strain ε_q at cavity wall during the expansion are shown in more detail for different overconsolidated soils. With the increase of OCR, the variation of η changes from monotonous increase to first increase and then decrease, which means that the soil change from single hardening behavior to hardening-softening behavior with the degree of overconsolidated

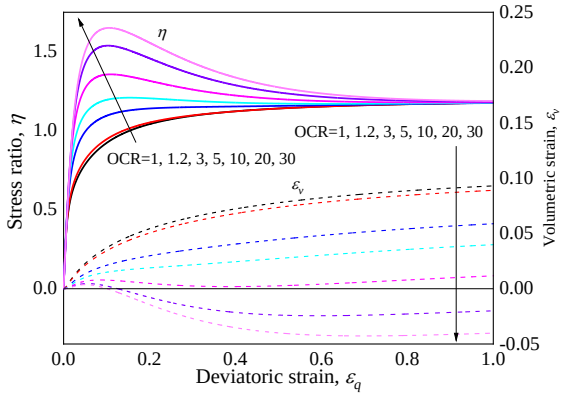

Fig. 7 Variations of stress ratio and volumetric strain with deviatoric strain at cavity wall

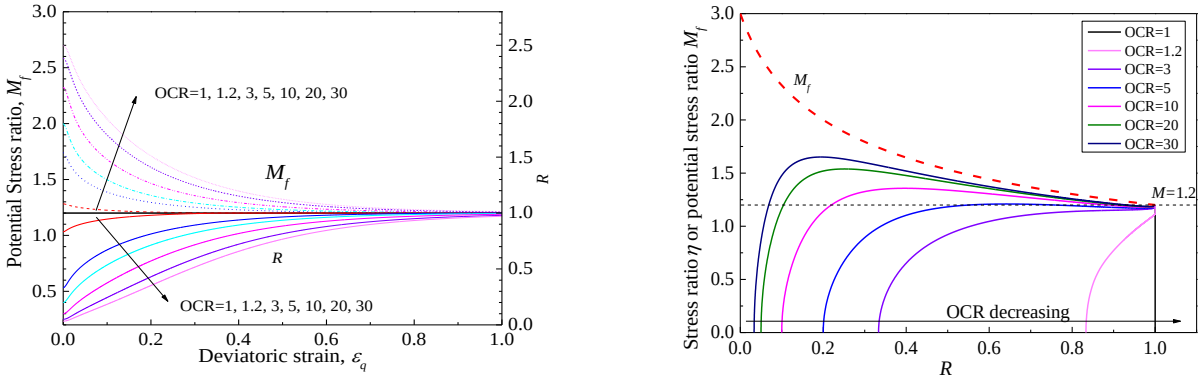

(a) Versus deviatoric strain (b) Versus overconsolidation parameter

Fig. 8 Variations of stress ratio or potential stress ratio at cavity wall during expansion

increasing. Due to the overconsolidated soils have experienced a greater stress level than current stress state in history, thus the contact between soil particles is much denser than normally consolidated soils. Therefore, the tight interaction between soil particles in the expansion process leads to the hardening-softening behavior of the soil, which also shown as the behavior of shear dilatancy-contraction in the volume of soil. Interestingly, with the drained cavity expansion process, the magnitude of ε_q when the soil reaches ultimate state exhibits large values ($\varepsilon_q = 0.5$~0.8 for different overconsolidated soils). It is probably due to there is no excess pore pressure produced in the soil around the cavity under the condition of drained expansion. Thus the soil is more difficult to reach the critical state, which is different from the undrained cavity expansion, i.e., the value of deviator strain is small when the soil reached to the critical state (Chen *et al.* 2020).

As shown in Fig. 7, for the normally consolidated soil and slightly overconsolidated soils with single hardening behavior, the volumetric strain at cavity wall always increases during cavity expansion, i.e., the soil always undergoes shear contraction, but for the overconsolidated soils, obvious shear dilatancy occurs in soil at cavity wall. It should be noted that the instant of soil behavior changes from shear dilatancy to shear contraction just corresponds to the point where the strain-hardening behavior transform to strain-softening behavior, which also shows that the results of present study can reasonably reflect the hardening/softening characteristics of overconsolidated soil during expansion.

4.4 Effect of OCR on potential peak strength behaviors

The peak strength behaviors of overconsolidated soils are reflected through the potential peak stress ratio M_f in the modified UH model. Recalling Fig. 6, the M_f path represents the stress path in the $p' - q$ plane of the potential peak stress ratio during the cavity wall expansion. As shown in the figure, the value of M_f at cavity wall gradually approaches the slope of the CSL with cavity expansion, and with the increase of OCR, the initial potential peak stress ratio also increases. To discuss the potential peak strength behaviors of soils more clearly, Fig. 8(a) plots the curves of potential peak stress ratio M_f and overconsolidation parameter R at cavity wall with deviatoric strain ε_q. For normally consolidated soils, the values of M_f and R stay constants which equal to 1.2 and 1 respectively; for different overconsolidated soils, the initial value of M_f increases with the increase of OCR, and all curves further decrease to $M_f = 1.2$ with cavity expansion. Simultaneously, the overconsolidation parameter R increases from the initial value of $1/OCR$ to $R = 1$, which indicates the soils at cavity wall gradually change from overconsolidated to normally consolidated during the cavity expansion.

The variation of stress ratio η or potential stress ratio M_f at cavity wall in the above process is shown in Fig. 8(b). with the increase of overconsolidation parameters, the stress ratio shows the same results as before, that is, the

normally consolidated soil and slightly overconsolidated soils represent single hardening behavior, while the moderately or heavily overconsolidated soils represent hardening-softening behavior, and the potential peak strength of overconsolidated soils increases with *OCR* increases. Moreover, the dotted line in Fig. 8(b) plots the M_f decreases monotonically with R increases, which corresponds to Eq. (7a). It should be noted that the maximum value of M_f is no more than 3 for extreme heavily overconsolidation, which is consistent with the experimental and theoretical results by other scholars (Yao *et al.* 2012, Schofield 2006), and it also shows the capabilities of present study on the cavity expansion problem in overconsolidated soils.

5. Conclusions

In this paper, a novel similarity solution is derived for a spherical cavity drained expansion in different overconsolidated soils, and the large strain deformation during the cavity expansion is considered in the solution technique by adopting logarithmic strain components. The exceptional modified UH model is selected to describe the unique mechanical behaviors of overconsolidated soils and the stress transformation method is adopted to reflect the 3D strength of soil. Considering the drained condition, the equations of the problem is summed up as an initial value problem of a set of ODEs, which is further solved by the commercial mathematics software MATLAB and the result was compared with the solution based on MCC model. Finally, the unique expansion behaviors in the overconsolidated clayey soils, such as the peak strength behavior, strain-hardening/softening and shear dilatancy behaviors, are discussed according to extensive parametric studies. The main conclusions are as follows:

• The results show that the present study can correctly reflect the stress distribution and shear contraction behavior of normally consolidated soils after expansion. By comparing with the MCC solution, the proposed method is not only verified under normally consolidated condition, the behavior of shear dilatancy of overconsolidated soil can interpreted by the present study more reasonably.

• For different overconsolidated soils, the potential peak strength of the soil at cavity wall gradually decreases with the expansion process, finally shows the characteristics as normally consolidated soil, and this disturbed range decreases with the value of *OCR* increases.

• The normally consolidated soil and slightly overconsolidated soils represent single hardening behavior and always undergo shear contraction during expansion, while the moderately or heavily overconsolidated soils exhibit strain hardening-softening behavior and the peak strength increase with the increase of *OCR* value.

The present method can be further used to evaluate the variation of the stress and strain state around the pile tip during pile installation, so as to calculate the shear strength of the soil at pile tip, and aims to guide the design of the vertical force during pile driving.

Acknowledgments

This work was supported by the Shanghai Sailing Program (Grant No. 19YF1436700). Financial support from this organization is gratefully acknowledged.

References

Bigoni, D. and Laudiero, F. (1989), "The quasi-static finite cavity expansion in a non-standard elasto-plastic medium", *Int. J. Mech. Sci.*, **31**(11/12), 825-837. https://doi.org/10.1016/0020-7403(89)90027-1.

Bishop, R.F., Hill, R. and Mott, N.F. (1945), "The theory of indentation and hardness tests", *Proc. Phys. Soc.*, **57**(3), 147. https://doi.org/10.1088/0959-5309/57/3/301.

Cao, L.F., Teh, C.I. and Chang, M.F. (2002), "Analysis of undrained cavity expansion in elasto-plastic soils with non-linear elasticity", *Int. J. Numer. Anal. Met. Geomech.*, **26**(1), 25-52. https://doi.org/10.1002/nag.189.

Carter, J.P., Randolph, M.F. and Wroth, C.P. (1979), "Stress and pore pressure changes in clay during and after the expansion of a cylindrical cavity", *Int. J. Numer. Anal. Met. Geomech.*, **3**(4), 305-322. https://doi.org/10.1002/nag.1610030402.

Chen, S.L. and Abousleiman, Y.N. (2013), "Exact drained solution for cylindrical cavity expansion in modified Cam Clay soil", *Géotechnique*, **63**(6), 510-517. https://doi.org/10.1680/geot.11.P.088.

Collins, I.F. and Stimpson, J.R. (1994), "Similarity solutions for drained and undrained cavity expansions in soils", *Géotechnique*, **44**(1), 21-34. https://doi.org/10.1680/geot.1994.44.1.21.

Coutinho, A.G.F.D. (1990), "Radial expansion of cylindrical cavities in sandy soils: Application to pressuremeter tests", *Can. Geotech. J.*, **27**(6), 737-748. https://doi.org/10.1139/t90-087.

Davis, R.O., Scott, R.F. and Mullenger, G. (1984), "Rapid expansion of a cylindrical cavity in a rate-type soil", *Int. J. Numer. Anal. Met. Geomech.*, **8**(2), 125-140. https://doi.org/10.1002/nag.1610080203.

Frydman, S. (2011), "Characterizing the geotechnical properties of natural, Israeli, partially cemented sands", *Geomech. Eng.*, **3**(4), 323-337. https://doi.org/10.12989/gae.2011.3.4.323.

Grevtsev, A. A. (2013), "Solution of one-dimensional problem of cavity expansion in soil within the framework of plastic-flow theory", *Soil Mech. Found. Eng.*, **49**(6), 209-218. https://doi.org/10.1007/s11204-013-9193-0.

Ha, T.G., Jang, I.S., Choo, Y.S. and Chung, C.K. (2014), "Evaluation of coefficient of consolidation for dilatory dissipation in piezocone test in overconsolidated cohesive soils", *KSCE J. Civ. Eng.*, **18**(2), 475-487. https://doi.org/10.1007/s12205-014-0191-1.

Hattab, M. and Hicher, P.Y. (2004), "Dilating behaviour of overconsolidated clay", *Soils Found.*, **44**(4), 27-40. https://doi.org/10.3208/sandf.44.4_27.

Hsieh, Y.M., Whittle, A.J. and Yu, H.S. (2002), "Interpretation of pressuremeter tests in sand using advanced soil model", *J. Geotech. Geoenviron. Eng.*, **128**(3), 274-278. https://doi.org/10.1061/(ASCE)1090-0241(2002)128:3(274).

Jocković, S. and Vukićević, M. (2017), "Bounding surface model for overconsolidated clays with new state parameter formulation of hardening rule", *Comput. Geotech.*, **83**, 16-29. https://doi.org/10.1016/j.compgeo.2016.10.013.

Jiang, X., Xiao, R., Zhang, M., Hu, W., Bai, Y. and Huang, B. (2020), "A laboratory investigation of steel to fly ash-based geopolymer paste bonding behavior after exposure to elevated temperatures", *Constr. Build. Mater.*, **254**, 119267. https://doi.org/10.1016/j.conbuildmat.2020.119267.

Jiang, X., Zhang, Y., Xiao, R., Polaczyk, P., Zhang, M., Hu, W., and Huang, B. (2020), "A comparative study on geopolymers synthesized by different classes of fly ash after exposure to

elevated temperatures", *J. Clean. Prod.*, **270**, 122500. https://doi.org/ 10.1016/j.jclepro.2020.122500.
Konkol, J. and Bałachowski, L. (2017), "Influence of installation effects on pile bearing capacity in cohesive soils–large deformation analysis via Finite Element Method", *Stud. Geotech. Mech.*, **39**(1), 27-38. https://doi.org/10.1515/sgem-2017-0003.
Li, C., Zou, J.F. and Li, L. (2019). "Elasto-plastic solution for cavity expansion problem in anisotropic and drained soil mass", *Geomech. Eng.*, **19**(6), 513-522. https://doi.org/10.12989/gae.2019.19.6.503.
Nguyen, B.P., Do, T.H. and Kim, Y.T. (2020), "Large-strain analysis of vertical drain-improved soft deposit consolidation considering smear zone, well resistance, and creep effects", *Comput. Geotech.*, **123**, 103602. https://doi.org/10.1016/j.compgeo.2020.103602.
Oka, F., Higo, Y. and Kimoto, S. (2002), "Effect of dilatancy on the strain localization of water-saturated elasto-viscoplastic soil", *Int. J. Solids Struct.*, **39**(13-14), 3625-3647. https://doi.org/10.1016/S0020-7683(02)00171-3.
Osinov, V.A. and Cudmani, R. (2001), "Theoretical investigation of the cavity expansion problem based on a hypoplasticity model", *Int. J. Numer. Anal. Met. Geomech.*, **25**(5), 473-495. https://doi.org/10.1002/nag.138.
Randolph, M.F. and Wroth, C.P. (1981), "Application of the failure state in undrained simple shear to the shaft capacity of driven piles", *Géotechnique*. **31**(1), 143-157. https://doi.org/10.1680/geot.1981.31.1.143.
Rao, P.P., Chen, Q., Li, L., Nimbalkar, S. and Cui, J. (2017), "Elastoplastic solution for spherical cavity expansion in modified Cam-clay soil under drained condition", *Int. J. Geomech.*, **17**(8), 06017005. https://doi.org/10.1061/(ASCE)GM.1943-5622.0000925.
Russell, A.R. and Khalili, N. (2002), "Drained cavity expansion in sands exhibiting particle crushing", *Int. J. Numer. Anal. Met. Geomech.*, **26**(4), 323-340. https://doi.org/10.1002/nag.203.
Schnaid, F., Kratz de Oliveira, L.A. and Gehling, W.Y.Y. (2004), "Unsaturated constitutive surfaces from pressuremeter tests", *J. Geotech. Geoenviron. Eng.*, **130**(2), 174-185. https://doi.org/10.1061/(ASCE)1090-0241(2004)130:2(174).
Schofield, A.N. (2006), "Interlocking, and peak and design strengths", *Géotechnique*, **56**(5), 357-358. https://doi.org/10.1680/geot.2006.56.5.357.
Sengun, E., Berilgen, M. and Incecik, M. (2014), "Effects of using different constitutive soil models for the cavity expansion problem", *Proceedings of the 8th European Conference on Numerical Methods in Geotechnical Engineering (NUMGE)*, Delft, The Netherlands, January.
Shuttle, D. and Jefferies, M. (2016), "Determining silt state from CPTu", *Geotech. Res.*, **3**(3), 90-118. https://doi.org/10.1680/jgere.16.00008.
Silvestri, V. and Abou-Samra, G. (2012), "Analytical solution for undrained plane strain expansion of a cylindrical cavity in modified cam clay", *Geomech. Eng.*, **4**(1), 19-37. https://doi.org/10.12989/gae.2012.4.1.019.
Sivasithamparam, N. and Castro, J. (2018), "Undrained expansion of a cylindrical cavity in clays with fabric anisotropy: Theoretical solution", *Acta Geotech.*, **13**(3), 729-746. https://doi.org/10.1007/s11440-017-0587-4.
Sun, D.A., Matsuoka, H., Yao, Y.P. and Ishii, H. (2004), "An anisotropic hardening elastoplastic model for clays and sands and its application to FE analysis", *Comput. Geotech.*, **31**(1), 37-46. https://doi.org/10.1016/j.compgeo.2003.11.003.
Vaziri, H.H. and Wang, X. (1993), "Theoretical solutions for the problem of a cylindrical cavity expansion in a Mohr-Coulomb material", *Comput. Struct.*, **48**(5), 961-962. https://doi.org/10.1016/0045-7949(93)90519-J.
Vesic, A.S. (1972), "Expansion of cavities in infinite soil mass", *J. Soil Mech. Found. Div.*, **98**(SM3), 265-269. https://ascelibrary.org/doi/abs/10.1061/JSFEAQ.0001740.
Vrakas, A. (2016), "Relationship between small and large strain solutions for general cavity expansion problems in elasto-plastic soils", *Comput. Geotech.*, **76**, 147-153. https://doi.org/10.1016/j.compgeo. 2016.03.005.
Wang, S. and Wu, W. (2021), "A simple hypoplastic model for overconsolidated clays", *Acta Geotech.*, **16**(1), 21-29. https://doi.org/10.1007/s11440-020-01000-z.
Wu X. and Xu Y. (2020), "Elasto-plastic solution for drained cavity expansion in over-consolidated soil incorporating three-dimensional unified hardening model", *Chin. J. Geotech. Eng.*, **42**(10), 1903-1913 (in Chinese). https://doi.org/10.11779/CJGE202010016.
Yang, C., Li, J. and Li, L. (2021), "Expansion responses of a cylindrical cavity in overconsolidated unsaturated soils: A semi-analytical elastoplastic solution", *Comput. Geotech.*, **130**, 103922. https://doi.org/10.1016/j.compgeo.2020.103922.
Yao, Y. P., Gao, Z., Zhao, J. and Wan, Z. (2012), "Modified UH model: Constitutive modeling of overconsolidated clays based on a parabolic Hvorslev envelope", *J. Geotech. Geoenviron. Eng.*, **138**(7), 860-868. https://doi.org/10.1061/(ASCE)GT.1943-5606.0000649.
Yazdani, H. and Toufigh, M.M. (2012), "Nonlinear consolidation of soft clays subjected to cyclic loading-Part I: Theory", *Geomech. Eng.*, **4**(4), 229-241. https://doi.org/10.12989/gae.2012.4.4.229.
Yu, H. S. (1992), "Expansion of a thick cylinder of soils", *Comput. Geotech.*, **14**, 21-41. https://doi.org/10.1016/0266-352X(92)90022-L.
Zhang, J., Li, L. and Sun, D.A. (2020), "Similarity solution for undrained cylindrical cavity contraction in anisotropic modified Cam-clay model soils", *Comput. Geotech.*, **120**, 103405. https://doi.org/10.1016/j.compgeo.2019.103405.
Zhou, H., Kong, G., Liu, H. and Laloui, L. (2018), "Similarity solution for cavity expansion in thermoplastic soil", *Int. J. Numer. Anal. Met. Geomech.*, **42**(2), 274-294. https://doi.org/10.1002/nag.2724.

JS

Notation

a_0	initial cavity radius
a	cavity radius
e_0	initial void ratio
λ	slopes of the isotropic compression line
κ	slopes of the isotropic swelling line
v_0	initial specific volume
v	specific volume
G	shear modulus of the soils
E	elastic modulus of the soils
v	Poisson's ratio
M	critical stress ratio
M_f	potential peak stress ratio
R	overconsolidation parameter
OCR	overconsolidation ratio
H	hardening parameter
K_p	plastic modulus
Λ	plastic scalar
r_0	initial radial coordinate of an arbitrary soil particle
r	radial coordinate of an arbitrary soil particle
p_0	initial mean stress
$\tilde{p}_x$	Shape parameters of reference yield surface
w	speed of soil particle at arbitrary radial coordinates
δ_{ij}	Kronecker's delta
σ_{ij}	stress components tensor in soils
σ_{a0}	initial internal cavity pressure
σ_a	internal cavity pressure
σ_{rin}, $\sigma_{\theta in}$	initial radial and circumferential stress components
S_i	deviatoric stress components
ε_{ij}^p	plastic strain components
ε_{ij}^e	elastic strain components
ε_r, ε_θ	total radial and circumferential strain components
ε_v^p	plastic volumetric strain

Appendix

The coefficients c_{ij} $(i,j=r,\theta)$ in Eq. (19) can calculated as:

$$c_{ij}=\frac{1}{3}+\left(\delta_{ij}-\frac{1}{3}\right)\frac{\ell_0}{\ell_\theta}+s_i\left[d_1+(3p'-\sigma_j')d_2+\frac{I_3}{\sigma_j'}d_3\right];\ i,j=r,\theta\# \tag{A1}$$

$$d_1=\frac{\ell_0}{I_1\ell_\theta}-\frac{2I_1\ell_0}{3\ell_\theta^3}+\frac{3\sqrt{6}I_2I_3\ell_0^2}{I_1\ell_\theta\psi(I_1I_2-9I_3)^2} \tag{A2}$$

$$d_2=\frac{\ell_0}{\ell_\theta^3}+\frac{3\sqrt{6}I_3\ell_0^2}{\ell_\theta\psi(I_1I_2-9I_3)^2} \tag{A3}$$

$$d_3=-\frac{3\sqrt{6}I_2\ell_0^2}{\ell_\theta\psi(I_1I_2-9I_3)^2} \tag{A4}$$

$$\psi=\sqrt{\frac{I_1I_2-I_3}{I_1I_2-9I_3}} \tag{A5}$$

where s_i $(i=r,\theta)$ is the deviatoric stress component, ℓ_0 and ℓ_θ are the position parameters of the curve of SMP criterion on the π plane, which are described in detail by Sun *et al.* (2004), and will not repeated in this paper.

The coefficients d_{11}, d_{12}, d_{21} and d_{22} in elastoplastic constitutive matrix are given as:

$$d_{11}=\frac{EK_{\mathrm{p}}\left[Eb_{22}+(1-v)K_{\mathrm{p}}\right)\right]}{B} \tag{A6}$$

$$d_{12}=\frac{EK_{\mathrm{p}}\left[-Eb_{12}+2vK_{\mathrm{p}}\right)\right]}{B} \tag{A7}$$

$$d_{21}=\frac{EK_{\mathrm{p}}\left[-Eb_{21}+vK_{\mathrm{p}}\right)\right]}{B} \tag{A8}$$

$$d_{22}=\frac{EK_{\mathrm{p}}\left[Eb_{11}+K_{\mathrm{p}}\right)\right]}{B} \tag{A9}$$

$$\begin{aligned}B=&K_{\mathrm{p}}^2(1-v-2v^2)\\&+EK_{\mathrm{p}}[(1-v)b_{11}+b_{22}\\&+v(b_{12}+2b_{21})]\\&+E^2(b_{11}b_{22}-b_{12}b_{21})\end{aligned} \tag{A10}$$

$$b_{11}=(c_{\mathrm{rr}}a_{\mathrm{r}}+2c_{\theta\mathrm{r}}a_\theta)a_{\mathrm{r}} \tag{A11}$$

$$b_{12}=2(c_{\mathrm{r}\theta}a_{\mathrm{r}}+2c_{\theta\theta}a_\theta)a_{\mathrm{r}} \tag{A12}$$

$$b_{21}=(c_{\mathrm{rr}}a_{\mathrm{r}}+2c_{\theta\mathrm{r}}a_\theta)a_\theta \tag{A13}$$

$$b_{22}=2(c_{\mathrm{r}\theta}a_{\mathrm{r}}+2c_{\theta\theta}a_\theta)a_\theta \tag{A14}$$